Journal of Colloid and Interface Science **253,** 315–328 (2002)
doi:10.1006/jcis.2002.8525

The Permeability of Synthetic Fractal Aggregates with Realistic Three-Dimensional Structure

Albert S. Kim* and Keith D. Stolzenbach†,[1]

*Department of Civil Engineering University of Hawaii at Manoa, Honolulu, Hawaii 96822; and †Department of Civil and Environmental Engineering University of California, Los Angeles, California 90095-1593

Received September 12, 2001; accepted June 6, 2002; published online August 27, 2002

The permeability of fractal porous aggregates with realistic three-dimensional structure is investigated theoretically using model aggregates composed of identical spherical primary particles. Synthetic aggregates are generated by several techniques, including a lattice-based method, simulation of aggregation by differential settling and turbulent shear, and the specification of simple cubic structures, resulting in aggregates characterized by the number of primary particles, solid fraction, characteristic radius, and fractal dimension. Stokesian dynamics is used to determine the total hydrodynamic force on and the distribution of velocity within an aggregate exposed to a uniform flow. The aggregate permeability is calculated by comparing these values with the total force and velocity distribution calculated from the Brinkman equation applied locally and to the entire aggregate using permeability expressions from the literature. The relationship between the aggregate permeability and solid fraction is found to be best predicted by permeability expressions based on cylindrical rather than spherical geometrical elements, the latter tending to underestimate the aggregate permeability significantly. The permeability expressions of Jackson and James or Davies provide good estimates of the force on and flow through porous aggregates of known structure. These relationships are used to identify a number of general characteristics of fractal aggregates.

Key Words: **permeability; fractal; aggregate.**

INTRODUCTION

The permeability of a suspended aggregate has many important consequences for physical, chemical, and biological interactions between the aggregate and its environment in engineered and natural systems (1, 2). For example, the settling speed of a porous aggregate will be greater than an impermeable aggregate of the same size and bulk density (3), and bacteria growing inside an aggregate will have greater access to dissolved nutrients (4).

A significant consequence of aggregate permeability is the relationship between the flow through the aggregate and the formation of the aggregate itself. The structure of an evolving aggregate will be affected by the permeability because the flow through the aggregate influences both the capture of new particles and the detachment of previously aggregated material. For example, the scavenging of fine particles by a faster-sinking aggregate or by aggregated material at the sediment–water interface will be more efficient if the smaller particles follow the flow into the aggregate and are filtered out in its interior (5, 6). Similarly, the flow distribution will determine if aggregate breakage occurs as a rupture of the large-scale aggregate structure or as erosion of attached particles near the outer surface of the aggregate (7, 8).

The permeability of porous aggregates has been studied both theoretically and experimentally (see next section). However, almost all theoretical analyses have used a porous sphere as a model aggregate, providing no information on the effect of realistic three-dimensional internal structure. The fragility and small size of suspended aggregates has made direct measurement of permeability virtually impossible; for this reason experimental studies have been limited to observations of bulk properties such as settling velocity, size, and average density from which permeability values are inferred using the porous sphere model.

This paper presents a theoretical analysis of the permeability of porous aggregates with realistic three-dimensional structure, using as a model system aggregates composed of identical spherical primary particles and assuming low Reynolds number flow. Synthetic model aggregates with systematically varying fractal dimensions are analyzed using Stokesian dynamics to determine the total hydrodynamic force on and the distribution of velocity within the aggregate. The aggregate permeability is calculated from the total force and the velocity distribution using the Brinkman equation applied locally and to the entire aggregate. The result of this analysis is the first comprehensive theoretical investigation of the permeability of aggregates with realistic three-dimensional structure.

BACKGROUND

Aggregate Structure

For the purposes of this study, aggregates are assumed to be composed of N_R primary spherical particles of identical radius a. It is now widely recognized that aggregates are fractal objects

[1] To whom correspondence should be addressed. Fax: (310) 206-2222. E-mail: stolzenb@ucla.edu.

0021-9797/02 $35.00

(9). The consequence of this fractal morphology is that N_R is related to the aggregate length scale R, by

$$N_R = A\left(\frac{R}{a}\right)^D, \quad [1]$$

where D is the fractal dimension of the aggregate and A is a prefactor that has been found empirically to be of order unity (10, 11). This definition of the fractal dimension D is related to the bulk properties of the aggregate (N_R and R) and does not require that the aggregate structure be self-similar at any scale, although all self-similar aggregates will satisfy Eq. [1]. Many studies use Eq. [1] applied to a population of aggregates of different size to determine D (e.g., 12). If measurements of the internal structure of an individual aggregate are available, the fractal dimension of can also be defined in terms of the slope of the two-point correlation function at the origin (9).

For an aggregate with realistic three-dimensional structure there are several choices for defining the length scale R. Assuming all primary particles have equal density, the average (orientation-independent) radius of gyration R_g is defined by

$$R_g^2 = \frac{\int_{V_a} r^2\phi(r)\,dV}{\int_{V_a}\phi(r)\,dV}, \quad [2]$$

where $\phi(r)$ is the local solid fraction and V_a is the whole aggregate volume. The "outer radius" R_f is defined by

$$R_f = \sqrt{\frac{D+2}{D}}R_g \quad [3]$$

and is always greater than the gyration radius (13, 14). Finally, if the aggregate length scale is defined as R_{max}, the distance from the center of mass to the outer edge of the outermost primary sphere, the average solid fraction of the aggregate ϕ_R is given by

$$\phi_R = N_R\left(\frac{a}{R_{max}}\right)^3. \quad [4]$$

Because of this convenient relationship to the definition of the aggregate solid fraction this study will use R_{max} as the characteristic length scale of the aggregate.

Aggregate Permeability

Aggregate permeability may be parameterized by a local intrinsic permeability κ defined empirically by Darcy's law for creeping flow through an isotropic porous medium,

$$\mathbf{q} = -\frac{\kappa}{\mu}\nabla p \quad [5]$$

where μ is the viscosity of fluid, p is the pressure, and $\mathbf{q}$ is the superficial velocity of the fluid. Brinkman formulated an empirical extension of Darcy's law to include the possibility of viscous stress terms in the local force balance (15):

$$\mathbf{q} = -\frac{\kappa}{\mu}(\nabla p - \mu\nabla^2\mathbf{q}). \quad [6]$$

TABLE 1
Analytical Permeability Functions for Porous Media with Solid Fraction ϕ and Primary Particle Radius a

Permeability function	Source
$\kappa_{DL} = \frac{2a^2}{9\phi} =$ dilute limit	Happel and Brenner (16)
$\kappa = \kappa_{DL}\frac{6 - 9\phi^{1/3} + 9\phi^{5/3} - 6\phi^2}{6 + 4\phi^{5/3}}$	Happel (17)
$\kappa = \kappa_{DL}\left(1 + \frac{3}{\sqrt{2}}\phi^{1/2} + \frac{135}{64}\phi\ln\phi + 16.456\phi + \cdots\right)$	Howells (18), Hinch (19), Kim and Russell (20)
$\kappa = \frac{\kappa_{DL}}{\xi(\alpha, \alpha/\phi^{1/3})} \quad \alpha = \frac{a}{\sqrt{\kappa}}$	Neale and Nader (21)
$\kappa = \kappa_{DL}\left(1 + \frac{3}{4}\phi\left(1 - \sqrt{\frac{8}{\phi} - 3}\right)\right)$	Brinkman (22)
$\kappa = \frac{a^2(1-\phi)^3}{9c\phi^2} \quad c \approx 5$	Kozeny–Carman equation (16)
$\kappa = \frac{3a^2}{20\phi}(-\ln\phi - 0.931 + O(\ln\phi)^{-1})$	Jackson and James (23)
$\kappa = \frac{a^2}{16\phi^{1.5}(1 + 56\phi^3)}$	Davies (24)

It is well understood that, for aggregates composed of primary particles of size a, the dimensionless permeability κ/a^2 generally depends only on the solid fraction of the media ϕ, but this dependence varies with the structure of the media in a way that is difficult to predict from first principles (16). The permeability formulations for porous media developed by various investigators are presented in Table 1 and compared as a function of volume fraction in Fig. 1. The dilute limit expression is derived for noninteracting spheres, i.e., assuming that the drag on each sphere is given by Stokes' Law. Many of the other expressions (17–22) are essentially theoretical modifications of the dilute limit force on a single sphere to account for the presence of other spheres, and all of these expressions converge to the dilute limit at solid fractions less than about 0.001–0.01. The expressions of Happel, Neale and Nader, and Brinkman are in close agreement for the entire range of solid fractions. However, the permeability predicted by the expressions of Howells, Hinch, and Kim and Russel diverge from the other models and become unrealistically constant for solid fractions greater than about 0.1.

The Kozeny–Carman equation is a semiempirical expression relating permeability of a granular close-packed porous medium to its volume fraction and hydrodynamic radius. It is generally valid for a porous medium with volume fraction greater than about 0.3 (16), so it agrees well with the expressions of

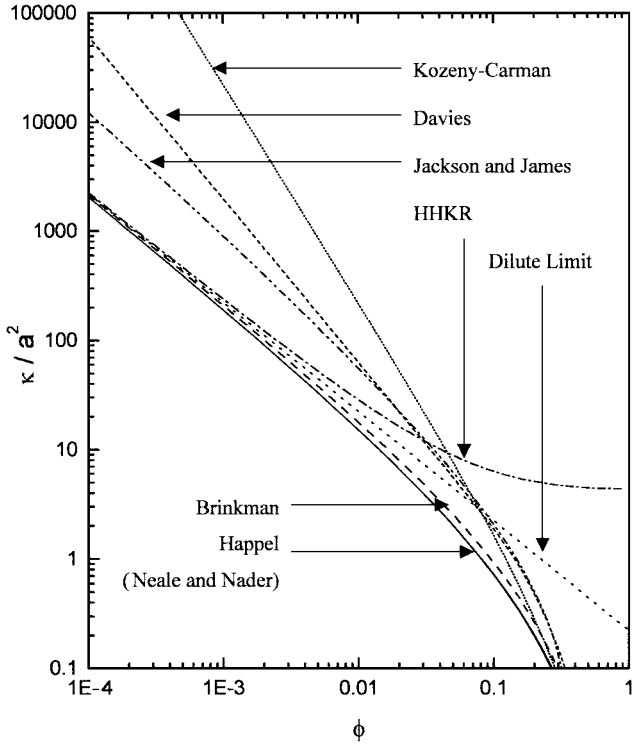

FIG. 1. Permeability as a function of volume fraction, based on the expressions given in Table 1. HHKR stands for the expressions of Howells (18), Hinch (19), Kim and Russel (20). The expression of Neale and Nader (21) is undistinguishable from that of Happel (17).

Happel and Neale and Nader at high volume fractions but deviates significantly from the dilute limit model at lower solid fractions.

The expressions of Jackson and James (23) and Davies (24) are designed to be applicable specifically to fibrous porous media. Jackson and James (23) obtained the theoretical permeability of long rods arranged in a periodic pattern within a unit cell. Using the results of Drummond and Tahir (25), they obtained an empirical permeability equation by adding the resistance of rods across the flow to that of rods aligned with the flow. The expressions of Jackson and James (23) agrees well with numerical results obtained by Higdon and Ford (26).

The empirical expression of Davies (24) is a fit to a large collection of permeability measurements on various media with fibrous structure for which the fibers were more realistically clustered together in comparison with the more ordered arrays analyzed by Jackson and James. The Davies expression predicts permeability values larger than that of Jackson and James, although it should be noted that the difference is significant only for relatively low solid fraction ($\phi < 0.001$) (see Fig. 1), and in fact the Davies expression represents most of the data compiled by Jackson and James rather well. It is interesting that both these formulations predict permeability values significantly higher than the sphere-based models, particularly at low solid fractions (see later discussion of this difference).

Flow Through and Force on a Spherical Aggregate in a Uniform Flow

A model system that has received much attention is the case of an idealized spherical aggregate of radius R held fixed in a uniform flow or sinking through a motionless fluid. Of interest is the resulting distribution of flow through and force on the aggregate. A number of previous investigators have developed theoretical solutions for the case of uniform permeability, using either Darcy's law (Eq. [5]) or the Brinkman equation (Eq. [6]) and appropriate boundary conditions at the surface of the sphere (see Neale *et al.* (3) for a review). The most widely used of these solutions is based on the Brinkman equation with continuity of stress and velocity at the sphere surface and assuming that the viscosity is everywhere the undisturbed fluid viscosity (15, 22). All kinematic properties of the system are determined by the value of a dimensionless parameter β, defined by

$$\beta = \frac{R}{\sqrt{\kappa}}. \qquad [7]$$

The hydrodynamic force F exerted on the sphere by the flow can be compared to the force on an impermeable sphere as follows:

$$F = \Omega(\beta) 6\pi\mu R U, \qquad [8]$$

where U is the external flow velocity and $\Omega(\beta)$ is a correction factor given by

$$\Omega = \frac{2\beta^2(1 - \tanh\beta/\beta)}{2\beta^2 + 3(1 - \tanh\beta/\beta)}. \qquad [9]$$

The correction factor is also the ratio of the settling velocity of a solid sphere to a permeable sphere of the same size and having the same total solid mass.

Solutions to this model problem can be used to illustrate the importance of the permeability on the flow around and through the sphere. Most cases fall into one of two categories determined by the relative values of R and $\sqrt{\kappa}$, the latter of which can be interpreted as the thickness of the flow field induced within the sphere by viscous shear stresses on the surface of the sphere (as opposed to the external pressure gradient, which tends to produce a relatively uniform flow within the sphere). For $\sqrt{\kappa} \gg R$ ($\beta \ll 1$) the permeability is so large that the fluid passes through the sphere without significant deflection and the drag force exerted on the aggregate by the flow is much smaller than the Stokes' Law value. For $\sqrt{\kappa} \ll R$ ($\beta \gg 1$), the permeability is so small that most of fluid in the path of the settling sphere is deflected around sphere and the drag is nearly equal to that given by Stokes' Law for an impermeable sphere. The flow capture "efficiency," defined as the ratio of the flow passing through the aggregate to the flow passing through an infinitely permeable sphere (as $\beta \to 0$) is also a function of β. Figures illustrating these flow patterns can be found in Stolzenbach (6) and Veerapaneni and Weisner (27).

Aggregates with radially varying permeability can be analyzed using a numerical solution to Brinkman's equation [6] applied to concentric shells of uniform permeability. This approach was used by Ooms *et al.* (28) to compute the permeability of polymer coils from sedimentation rates. Details of this type of calculation are given by Veerapaneni and Wiesner (27), who investigated the relationship between the fractal dimension of a permeable aggregate and the resulting values of $\Omega(\beta)$ and the flow capture efficiency. Although a review of permeability relationships is presented in this paper, most of the calculations are performed using only the Happel permeability expression (see Table 1) in the range of solid fractions where it is very close to the dilute limit (see Fig. 1).

Numerical Calculation of the Force and Flow Distribution

A number of previous investigators have used numerical solutions to the fundamental low Reynolds number flow equations to analyze the flow and force distributions in synthetically generated aggregates formed from monodisperse primary particles (see Filippov (29) for a recent review). In the Stokesian dynamics method the essential approximation is to first form the grand mobility matrix of the system using a limited number of terms in the series representing the pairwise far-field interactions. The actual calculations are performed using resistance matrices calculated by inverting the grand mobility matrix and, where appropriate, adding near field lubrication terms based on pairwise resistance formulas truncated to the same order of approximation as the original mobility series (30).

A number of studies have used Stokesian dynamics to investigate porous aggregates. The force on linear chains of spheres and cubic arrays of nontouching spheres predicted by the Stokesian dynamics method of Durlofsky *et al.* (31) is in good agreement with numerical solutions of Ganatos *et al.* (32) and Hassonjee *et al.* (33). Durlofsky and Brady (34) demonstrated that Stokesian dynamics calculations yield force–velocity relationships consistent with the Brinkman equation [6]. Bossis *et al.* (35) used Stokesian dynamics to analyze the force on synthetic aggregates exposed to a uniform external flow. They noted that the drag averaged over all possible orientations of the aggregate with respect to the external flow could be obtained directly from the trace of the resistance tensor. In addition, they concluded that for aggregates with a large number of particles with positions fixed relative to each other, the inclusion of the near-field lubrication terms led to a significant overestimation of the drag on the aggregate because the pairwise lubrication terms added to the resistance matrix in the standard Stokesian dynamics formulation did not account for the reduction of the external velocity within the aggregate. They showed that leaving out the lubrication terms was a more reasonable approximation, particularly given the small near-field contributions for particles without relative motion. Vitthal and Sharma (36) used Stokesian dynamics to compute the filtration of small particles by larger close-packed collectors. This study was characterized also by its use of three-particle mobility functions derived by Mazur and Van Saarloos (37) as a way of obtaining a more accurate initial mobility matrix.

Experimental Studies

There are few experimental studies of porous aggregates. Matsumoto and Suganuma (38) observed the settling velocity of artificial porous aggregates and used Eq. [9] to compute the implied value of the aggregate permeability. Their results agreed well with the empirical correlation of Davies (24). Similar observations and analyses were made by Masaliyah and Polikar (39) and Li and Ganczarczyk (40), but with less definitive quantitative results. Lasso and Weidman (41) observed the settling velocity of close-packed conglomerates, but interpreted their results in terms of a hydrodynamic radius rather than an effective permeability in order to avoid invoking the Brinkman model.

Johnson *et al.* (42) and Li and Logan (43) observed the settling velocities of individual aggregates formed from primary particles of known size and density. The overall solid fraction and bulk density of each aggregate was determined by counting the particles in aggregates retrieved after being settled and using an estimated aggregate size based on the observed projected area of the aggregate at rest after settling. Their results indicate that the aggregates settled substantially faster (2 to 20 times faster in Johnson *et al.* (42) and 1.5 to 7 times faster in Li and Logan (43)) than impermeable spheres with the same bulk density, corresponding to values of $\Omega(\beta)$ roughly between 0.05 and 0.5. They were unable to reconcile these results with any of the permeability expressions in Table 1, all of which predicted a smaller difference between the settling velocities of permeable and impermeable spheres (values of $\Omega(\beta)$ closer to unity). This discrepancy corresponds to an equivalent underestimation of the permeability of these aggregates when the permeability is calculated using the actual primary particle size (the quantity a in the normalized permeability κ/a^2). These investigators have attempted to resolve this by hypothesizing that the particle size used in the permeability relationship should be effectively larger than the primary particles (see Li and Logan (44) for the most recent discussion of this point). According to their analysis, the effective particle size represents clusters of primary particles, resulting from the nonuniform distribution of the primary particles in a fractal aggregate, that shelter each other from the flow and are thus relatively impermeable. The increase in the effective particle size results in a corresponding increase in the permeability of the aggregate. The validity of this explanation for fractal aggregates is discussed later in this paper.

METHODS

In this section, we present the methods use to generate synthetic fractal aggregates, to characterize the structure of the aggregates, to compute the distribution of force on and flow through the aggregates, and to derive the aggregate permeability.

TABLE 2
Properties of Synthetic Aggregates

Aggregate type	N_R	ϕ_R	D	R_{max} a	R_g a	R_f a	R_{h-SD} a	R_{h-D} a	R_{h-JJ} a	R_{h-H} a	R_{h-KC} a	n_p	n_l	k
Lattice-based	13	0.18	2.33	4.2	2.3	3.2	2.8	3.2	3.1	3.5		13	3	1
	169	0.076	2.33	13.0	7.5	10.2	8.8	9.6	9.5	10.9		13	3	2
	2197	0.035	2.33	39.7	22.5	30.7	26.9	29.6	29.8	31.8		13	3	3
	13	0.12	1.85	4.8	2.6	3.8	3.1	3.3	3.2	3.9		13	4	1
	169	0.027	1.85	18.4	10.9	15.8	11.8	11.7	11.8	14.1		13	4	2
	2197	0.0056	1.85	73.1	43.8	63.2	46.2	48.7	51.4	59.3		13	4	3
	13	0.049	1.59	6.4	3.7	5.6	3.5	3.5	3.4	4.6		13	5	1
	169	0.0052	1.59	32.0	18.8	28.2	15.6	14.4	15.8	21.7		13	5	2
	2197	0.00054	1.59	159.8	93.9	141.0	73.5	69.2	91.0	121.1		13	5	3
Differential settling	300	0.023	1.98	26.0	13.6	19.3	14.9	15.0	15.1	17.5				
Turbulent shear	300	0.012	1.48	29.5	16.2	25.0	17.7	16.7	17.2	21.1				
Cubic closed-packed	64	0.27	3.00	6.2	3.9	5.0	4.8	5.7			5.8		4	
	216	0.24	3.00	9.7	5.9	7.6	7.5	8.5			8.4		6	
	512	0.23	3.00	13.1	7.9	10.2	10.2	10.0			11.3		8	
	1000	0.22	3.00	16.6	9.9	12.8	12.9	12.7			14.1		10	

Note. See text for definitions of N_R, ϕ_R, D, a, R_{max}, R_g, R_f, R_h, n_p, n_l, and k. The subscript on R_h denotes the source of the analysis. SD, Stokesian dynamics. All others relate to the shell analysis using the permeability function used with the Brinkman equation: D, Davies; JJ, Jackson and James; H, Happel; KC, Kozeny–Carmen.

Synthetic Aggregate Generation

Three types of aggregates were generated in this study (see Table 2 for a summary of aggregate properties):

Random lattice-based aggregates (13). These aggregates are composed of subunits consisting of simple-cubic latices with n_l^3 possible locations within which n_p primary spheres are arranged in a random but connected configuration, including at least two spheres on an outer face to provide connections to adjacent subunits. Aggregates are synthesized with k generations with $k = 2$ corresponding to n_p of the subunits arranged within a larger cubic lattice according to the same rules. Generation $k = 3$ is constructed with n_p of the $k = 2$ structures, and so on. The theoretical fractal dimension for these aggregates, corresponding to Eq. [1] with $A = 1$, is

$$D = \frac{\ln n_p}{\ln n_l}, \qquad [10]$$

where the minimum value of n_p is limited by $3n_l - 2$. Examples of lattice aggregates generated by this method are shown in Fig. 2.

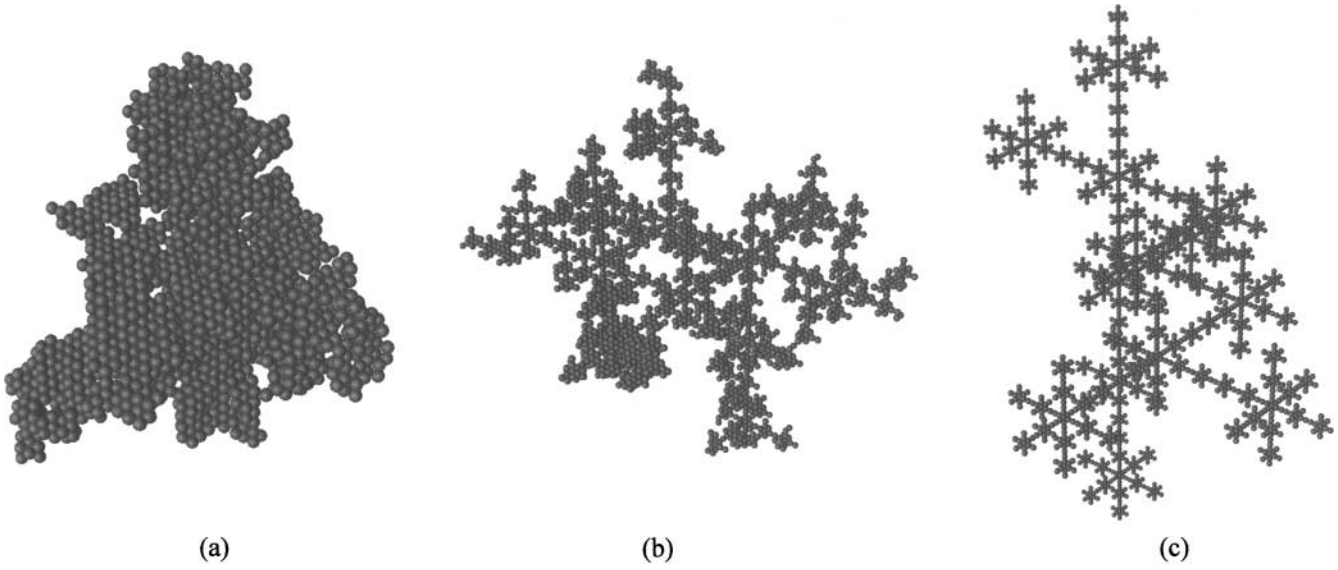

FIG. 2. Examples of synthetic lattice aggregates, all of third generation ($k = 3$) with $N_R = 2197$ and $n_p = 13$ (see Table 2). (a) $n_l = 3$ and $D = 2.33$, (b) $n_l = 4$ and $D = 1.85$, (c) $n_l = 5$ and $D = 1.59$.

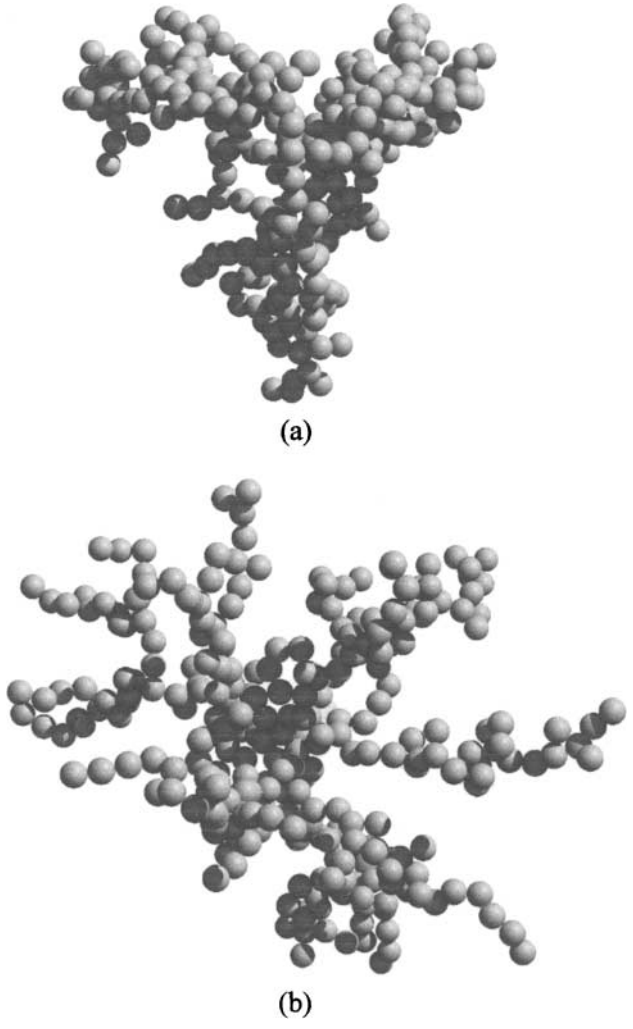

FIG. 3. Aggregates with $N_R = 300$ generated using Stokesian dynamics for (a) differential settling and (b) turbulent shear (Kim and Stolzenbach, in preparation).

Aggregates generated by simulation of differential settling and shear flow. As a part of a related study Stokesian dynamics techniques were used to simulate the formation of aggregates by these two collision mechanisms (45) (Kim and Stolzenbach, in preparation). Two aggregates with $N_R = 300$, one representing each of these processes, were analyzed by this study (see Fig. 3). The fractal dimensions of these aggregates were determined from the slope of the two-point correlation function at the origin (9).

Simple cubic structures with n_l^3 primary spheres for $n_l = 4$, 6, 8, and 10. All of these aggregates have a fractal dimension $D = 3$.

Calculation of the Drag Force on an Aggregate Using Stokesian Dynamics

The drag force experienced by an aggregate is calculated by the method used in Stokesian dynamics (30, 31). The hydrodynamic forces F, torques T, and the stresses S on the particles are generally related to the translational velocities U, rotational velocities ω, relative to the external linear fields U^∞ and ω^∞, respectively, by

$$\begin{bmatrix} U - U^\infty \\ \omega - \omega^\infty \\ -E^\infty \end{bmatrix} = \begin{bmatrix} \mathbf{M}_{UF} & \mathbf{M}_{\Omega F} & \mathbf{M}_{EF} \\ \mathbf{M}_{UT} & \mathbf{M}_{\Omega T} & \mathbf{M}_{ET} \\ \mathbf{M}_{US} & \mathbf{M}_{\Omega S} & \mathbf{M}_{ES} \end{bmatrix} \begin{bmatrix} F \\ T \\ S \end{bmatrix}, \quad [11]$$

in which $\mathbf{M}$ is the mobility matrix and E^∞ is the rate of strain of the imposed flow field. For N particles, F, T, $U - U^\infty$, and $\omega - \omega^\infty$ are vectors of dimension $3N$ and, the symmetric and traceless part of both $S = (S_{11}, S_{12}, S_{13}, S_{23}, S_{22})$ and $E^\infty = (E^\infty_{11} - E^\infty_{33}, 2E^\infty_{12}, 2E^\infty_{13}, 2E^\infty_{23}, E^\infty_{22} - E^\infty_{33})$ have dimension $5N$. The resistance matrix $\mathbf{R}$, the inverse of the mobility matrix $\mathbf{M}$, is defined by

$$\begin{bmatrix} F \\ T \\ S \end{bmatrix} = \begin{bmatrix} \mathbf{R}_{FU} & \mathbf{R}_{F\Omega} & \mathbf{R}_{FE} \\ \mathbf{R}_{TU} & \mathbf{R}_{T\Omega} & \mathbf{R}_{TE} \\ \mathbf{R}_{SU} & \mathbf{R}_{S\Omega} & \mathbf{R}_{SE} \end{bmatrix} \begin{bmatrix} U - U^\infty \\ \omega - \omega^\infty \\ -E^\infty \end{bmatrix}. \quad [12]$$

In the original Stokesian dynamics simulation method (30), the elements of a grand resistance matrix $\mathbf{R}$ in Eq. [12] are calculated as the inverse of the grand mobility matrix $\mathbf{M}^{-1}$, determined using mobility coefficients calculated separately for each pair of spheres to a given order of approximation. For the general case of many moving spheres, pairwise lubrication resistance terms were added to $\mathbf{M}^{-1}$ in a consistent manner. However, because lubrication is not important when all the particles move at the same velocity (46), lubrication terms are not included in the calculation of the drag on an aggregate. As mentioned earlier, the addition of lubrication terms in grand resistance matrix can lead to a significant overestimation of the drag force for large dense aggregate for which the velocity field is screened inside an aggregate (35).

The set of linear equations represented by [11] and [12] can be modified and simplified to calculate the permeability of a rigid aggregate composed of N spherical rigid particles of radius a, held motionless in an external flow with a uniform velocity U^∞. In this case $U = \omega = E^\infty = 0$, and Eqs. [11] and [12] can be written as

$$[F] = [\mathbf{R}_{FU}][-U^\infty] \quad [13]$$

$$[-U^\infty] = [\mathbf{M}_{FU}][F], \quad [14]$$

respectively. In this formulation the grand resistance matrix and the grand mobility matrix are reduced from $11N \times 11N$ to $3N \times 3N$.

The total hydrodynamic force on the aggregate given by Eq. [13] depends on the orientation of the external flow with respect to the aggregate structure. However, the average force $\bar{F}$, corresponding to an average over all possible orientations of the aggregate relative to the external flow, will be given by the trace of the resistance matrix coupling the force and translational

velocity (35)

$$\bar{F} = U^{\infty}\frac{1}{3}\sum_{i=1}^{N}\sum_{j=1}^{N}\mathrm{Tr}\left(\mathbf{R}_{\mathrm{FU}}^{ij}\right). \quad [15]$$

An average hydrodynamic radius may then be expressed as

$$\frac{R_{\mathrm{h}}}{a} = \frac{\bar{F}}{6\pi\mu a U^{\infty}}, \quad [16]$$

where μ is the viscosity of ambient fluid. The mathematical operations to obtain R_{h} consist of the inversion of a $3N \times 3N$ grand mobility matrix and the computation of its trace. This calculation was programmed in parallel mode using the **pdgetri** and **pdgetrf** subroutines of ScaLAPACK (47) in a Linux cluster composed of four nodes.

It is interesting to note that Eq. [15] gives the average force corresponding to a constant value of U^{∞}. It is also possible to specify a constant force F and, using Eq. [14], determine that the average velocity $\overline{U^{\infty}}$ corresponding to all possible orientations of the force F is given by

$$\overline{U^{\infty}} = \frac{F}{3}\left(\frac{1}{\mathbf{R}_1} + \frac{1}{\mathbf{R}_2} + \frac{1}{\mathbf{R}_3}\right), \quad [17]$$

where $\mathbf{R}_1$, $\mathbf{R}_2$, and $\mathbf{R}_3$ are the principal values of the resistance matrix (16). The average force corresponding to $\overline{U^{\infty}}$ may then be defined as

$$\bar{F} = \bar{\mathbf{R}}\overline{U^{\infty}}, \quad [18]$$

where $\frac{1}{\bar{\mathbf{R}}} = \frac{1}{3}(\frac{1}{\mathbf{R}_1} + \frac{1}{\mathbf{R}_2} + \frac{1}{\mathbf{R}_3})$. The aggregates used in this study are relatively spherical and the diagonal elements in the both resistance and mobility matrices are nearly equal and are larger than the off-diagonal elements. The result is that the two methods of averaging described above give essentially identical results for the quantity $\bar{F}$. The results of this study are based on the force given by Eq. [15] as this corresponds to the force computed analytically using the Brinkman equation (see below).

Calculation of the Flow Field through the Aggregate Using Stokesian Dynamics

The Stokesian dynamics relationships (Eqs. [11] and [12]) do not yield the fluid velocity directly. Accordingly, the fluid velocity inside the aggregate with readius $R_{\max}$ was obtained indirectly by using these relationships to calculate the velocity of a small "tracer" particle of radius $10^{-3}a$ in a plane passing through the center of mass of the aggregate perpendicular to the direction of the approaching flow. At a given dimensionless distance $r/R_{\max}$, the velocity of the tracer particle was calculated at 36 points by increasing the azimuth angle by $\pi/18$ if the tracer particle did not overlap any of the primary particles. The flow velocity was approximated by averaging the velocities of the tracer particle of all the points at a dimensionless distance in a plane. Since aggregates do not have perfect spherical symmetry, the final velocity was determined as the average of values obtained using three orthogonal planes.

Calculation of the Force and Flow within a Spherical Aggregate Using Brinkman's Equation

The velocity distributions within the aggregates considered by this study were also analyzed using Brinkman's equation [6] applied to the case of an aggregate held stationary in a uniform flow with velocity U^{∞}. In this analysis each aggregate was represented as a spherically symmetrical structure with a radially varying solid fraction $\phi(r)$, determined from the actual aggregate structure by averaging the mass within a shell at a given radius. A corresponding radially varying permeability $\kappa(r)$ was defined using one of the permeability expressions reviewed in the foregoing section.

A solution was obtained by considering the general analytical solution to Brinkman's equation within a spherical shell extending from r to $r + \Delta r$. An additional general solution governs the flow field outside the aggregate, approaching a uniform velocity U^{∞} at large distances from the aggregate. The coefficients determining the solution within each shell were then calculated by solving a system of linear equations formed by requiring continuity of velocity and stress between adjacent shells and between the outermost shell and the external flow field. The force and flow distribution within the aggregate and the total force on the aggregate are then easily obtained from the values of the coefficients. This method is described in greater detail in Veerapaneni and Wiesner (27).

RESULTS

Verification of Force Calculations

Three cases were chosen to test the method described to compute the force on a synthetic aggregate. Durlofsky *et al.* (31) calculated the drag coefficient for four identical particles at the corners of a square of side L sinking perpendicular to the plane of the square using the FT version of Stokesian dynamics with the lubrication interaction. They specified the gravitational forces acting on each particle and calculated the resulting sinking velocities. In their approach the particles are allowed to rotate as they sink. Figure 4 shows the drag coefficient for the four particles calculated by Durlofsky's approach and the method used in this study. Even if the rotation of each particle is prohibited as in this study, the drag coefficients calculated by both methods are almost identical, showing that the pairwise lubrication interaction does not play an important role when the center-to-center distance between two particles is greater than the four sphere radii.

Hassonjee *et al.* (33) also provided the hydrodynamic drag coefficients of 64 particles that are rigidly held as well as rotating in a uniform flow at the corners of $4 \times 4 \times 4$ simple cubic array for which the center-to-center distance between the nearest two particles is 16.12 sphere radii. They specified the velocity of a

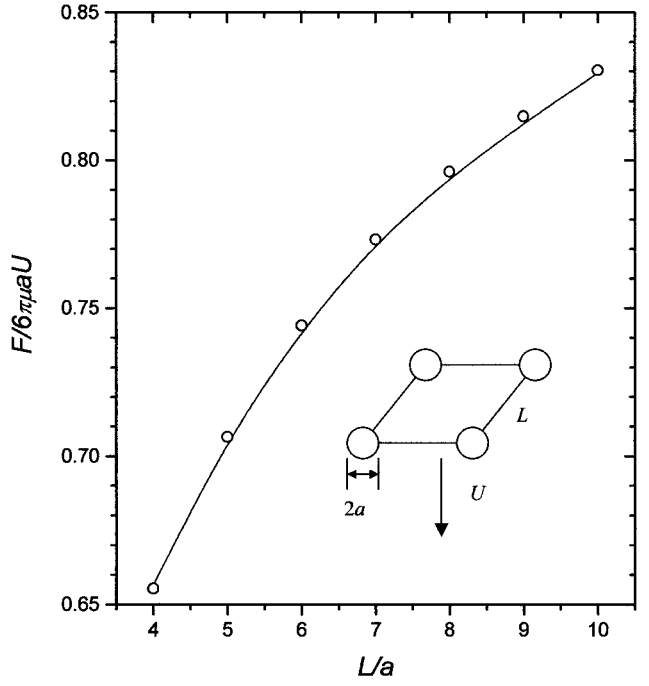

FIG. 4. The drag coefficient $F/6\pi\mu aU$ calculated by Stokesian dynamics for four identical spheres at the corners of a square of side L sinking perpendicular to the plane of the square. The solid line is the calculation of Durlofsky *et al.* (31), and the open circles are the Stokesian dynamics simulation of this work.

uniform upflow and calculated the forces acting on each of the 64 particles, from which they calculated an average drag coefficient of 0.369775. The method of this study gives 0.369838, corresponding to a relative error of 0.017%.

Filippov (29) used a multipole expansion technique to calculate the force on hexagonal-closed-packed aggregates of primary spheres and found that his results compared favorably to values measured by Lasso and Weidman (41) and obtained by Cichocki and Hinsen (48) using another higher-order analytical technique. Hydrodynamic radii calculated using the methods of this study are within 5–13% of the other estimates (see Table 3).

TABLE 3

Dimensionless Hydrodynamic Radii of Aggregates with Hexagonally Closed-Packed Structure Measured by Lasso and Weidman (L&W) (41), and Calculated by Cichocki and Hinsen (C&H) (48), Filippov (29), and This Study

N_R	L&W	C&H	Filippov	This study
3	1.195	1.1595	1.1958	1.1094
5	1.095	1.0783	1.0778	0.9637
13	1.143	1.1356	1.1342	1.2791
57	1.131	1.1440	1.1372	1.0772

Note. Results for L&W, C&H, and Filippov are taken from Filippov (29). The dimensionless hydrodynamic radius is defined by Eq. [56] in Filippov (29) and is equal to $N_R^{1/3}$.

Hydrodynamic Radius of Synthetic Aggregates

The average hydrodynamic radii calculated by Stokesian dynamics and by the Brinkman equation are summarized in Table 2 and Fig. 5. For most aggregates the Brinkman equations were solved using three different permeability formulations: Happel, Jackson and James, and Davies. For the cubic-closed packed aggregates the Kozeny–Carman relationship was also used.

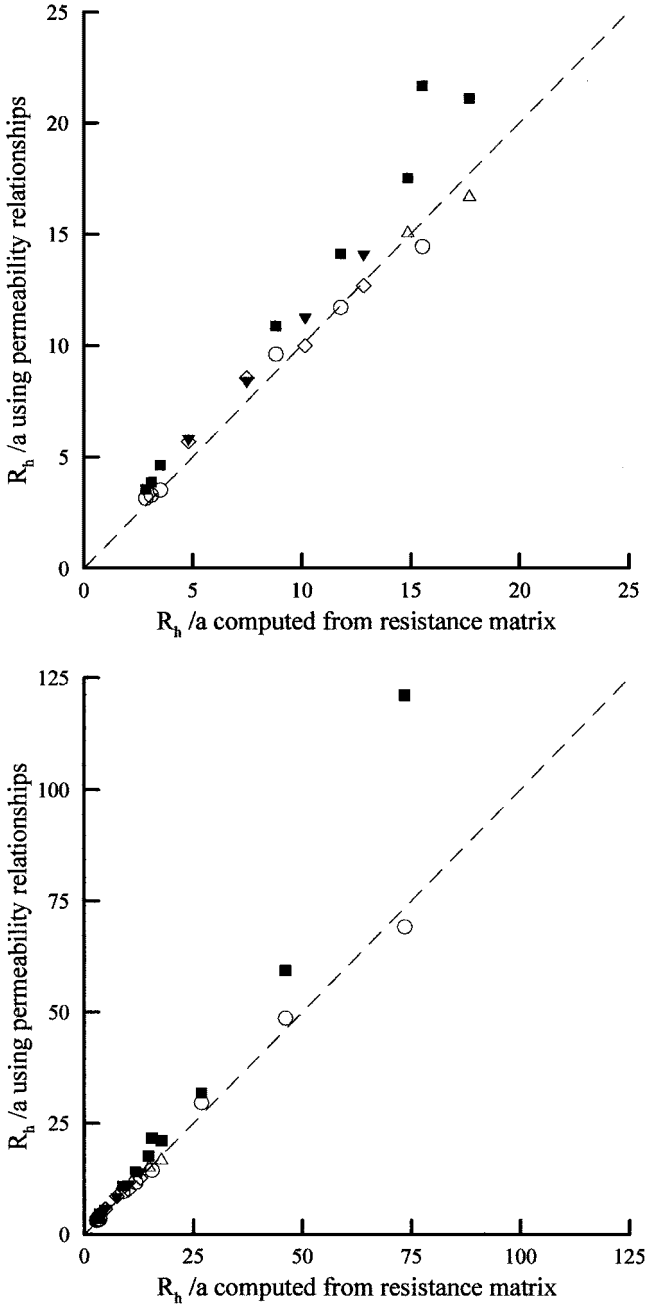

FIG. 5. Values of $R_{h/a}$ calculated from the Stokesian dynamics resistance matrix and from the Brinkman equation applied to a spherically symmetric aggregate using a specific permeability expression. Davies: lattice, ○; shear/gravity, △; cubic, ◇; Happel lattice and shear/gravity, ■; Kozeny-Carman cubic, ▼.

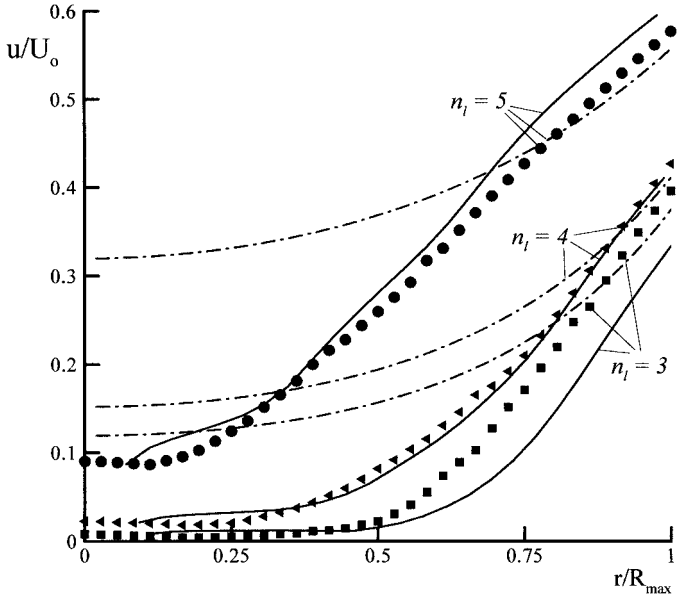

FIG. 6. Velocity distribution within lattice aggregates of second generation ($k = 2$) using the Stokesian dynamics simulation (solid symbols), the Brinkman equation in conjunction with the Davies permeability expression (solid lines), and the theoretical solution for a uniform sphere with the same average solid fraction and using the Davies permeability expression (dashed-dot lines).

Velocity Distribution

The velocity distribution within an aggregate was calculated for three of the lattice-based cases ($n_1 = 3$, 4, and 5 for $k = 2$) using the Stokesian dynamics simulation and the Brinkman equation in conjunction with the Davies correlation (Fig. 6). Also shown for comparison are the theoretical velocity distributions corresponding to an aggregate of uniform permeability set equal to the permeability calculated with the Davies correlation using the average solid fraction for the aggregate.

DISCUSSION

Accuracy of Simulation Method

The hydrodynamic forces calculated with Stokesian dynamics are generally within 10% of the values obtained using higher-order methods that may be less feasible for aggregates with a large number of primary particles. This difference is clearly the result of the relatively small number of terms represented in constructing the pairwise mobility matrix that is the starting point for the Stokesian dynamics calculations. This level of accuracy is found to be acceptable for the purposes of this study, i.e., to evaluate alternative permeability relationships by comparing hydrodynamic force values for aggregates with real three-dimensional structure and a large number of primary particles.

Permeability Relationships

An important finding of this study is that a permeability relationship based on the local solid volume fraction is adequate to describe the force on and flow within the aggregate, independent of overall structure of the aggregate, i.e., the fractal dimension (see Figs. 5 and 6). It is clear from the results presented in Fig. 5 that the total hydrodynamic force calculated using a permeability based on either the Jackson and James or the Davies relationships applied to synthetic fractal aggregates with fractal dimensions between 1.45 and 3.0 are in good agreement with the total force calculated using Stokesian dynamics. It is not surprising that the Jackson and James and Davies results are relatively indistinguishable given the similarity in the values of permeability for a given solid fraction, particularly for higher solid fractions. The Davies relationship provides a good estimate of the force on cubic-close-packed aggregates with $D = 3$.

Flow distributions within the fractal aggregates are also well represented by the Davies relationship (Fig. 6), although there is some trend in the agreement with the size of the aggregate. It is clear that the uniform permeability assumption greatly overestimates the magnitude of the flow through the interior of the aggregate, although it is interesting that relatively good agreement is obtained near the outer edge of the aggregate. This result is a consequence of the radial distribution of the solid fraction given by Eq. [20]. For $D < 3$ the solid fraction in the center of the simulated aggregates is larger than the bulk solid fraction ϕ_R and thus less permeable to flow in this region. The solid fraction in the outer region of the aggregate is closer to the bulk value, making the theoretical distribution a better representation for this region. For the aggregate, most of the contribution to the volumetric flow rate is from the flow in the region $r/R_{max} > 1 - \beta^{-1}$.

Another finding of this study is that the permeability relationships based on cells surrounding spherical rather than cylindrical unit elements overestimate the force on the fractal aggregates (Fig. 5). Because of the general dependence of the force on aggregate permeability (see next section), this difference in force may correspond to a significant, even order-of-magnitude, underestimation of the aggregate permeability. This finding is consistent with the relative permeability values predicted by the Davies and, for example, Happel relationships, the latter being lower, particularly for small solid fractions. The physical reason for this difference is that the spherical unit cell relationships inherently minimize the interactions between neighboring particles, in particular the likelihood that one particle will shelter another from the force of the flow passing through the aggregate. In fact, for solid fractions below the closed-packed range, the spherical-cell formulations correspond to a system of unconnected particles, more characteristic of a suspension than an aggregate. Real aggregates with low solid fractions consist of particles arranged in connected chains that are better represented by cylindrical unit-cell relationships such as Jackson and James or empirical fits to data based on fibrous porous media such as Davies.

The Ideal Aggregate Model

There have been very few measurements of the internal structure of individual real aggregates, particularly in aquatic

systems. Nevertheless, several studies (8, 27) have assumed that the internal structure of an aggregate has the same form as Eq. [1]; i.e., the number of primary particles $N(r)$ within a radial distance r, defined here as the distance from the center of mass of the aggregate (assuming the primary particles all have the same density), varies according to

$$N(r) = A\left(\frac{r}{a}\right)^{D}. \qquad [19]$$

If $N(r)$ is distributed according to Eq. [19] with $A = 1$, the local $\phi(r)$ and average $\bar{\phi}(r)$ volume fractions then vary radially according to

$$\phi(r) = \frac{\frac{4\pi}{3}a^3}{4\pi r^2}\frac{\mathrm{d}N(r)}{\mathrm{d}r} = \frac{D}{3}\left(\frac{r}{a}\right)^{D-3} \qquad [20]$$

$$\bar{\phi}(r) = \frac{\frac{4\pi}{3}a^3}{\frac{4\pi}{3}r^3}N(r) = \left(\frac{r}{a}\right)^{D-3}, \qquad [21]$$

where $\bar{\phi}(R) = \phi_R$. For ideal aggregates the outer radius R_f is equal to the maximum radius R_{max}.

This section will investigate the permeability-related properties of an aggregate with the ideal fractal structure given by Eq. [19] with a prefactor $A = 1$ and with a bulk permeability ϕ_R given by Eq. [4]. For such an aggregate the structural parameters R_{max}/a and N_R are completely determined by the values of D and ϕ_R:

$$\frac{R_{max}}{a} = \phi_R^{\frac{1}{D-3}} \qquad [22]$$

$$N_R = \phi_R^{\frac{D}{D-3}}. \qquad [23]$$

These fundamental relationships illustrate the inherent constraints on investigations of how other features of the aggregate, such as permeability, vary with fractal dimension. For example, if solid fraction is to be kept constant, changes in the fractal dimension must be accompanied by corresponding changes in both the size of the aggregate (relative to the primary particles) and the total number of particles.

The preceding sections demonstrate that either the Jackson and James or the Davies permeability model can be used as the basis for a calculation of the distributed and total force on and flow through a porous aggregate of known structure. For $\phi < 0.1$, the Davies expression may be approximated by

$$\frac{\kappa}{a^2} \approx \frac{1}{16\phi^{1.5}}. \qquad [24]$$

This expression and Eq. [20] are used to plot the distribution of local permeability within an ideal fractal aggregate, normalized by $\kappa(\phi_R)$, the permeability associated with the bulk solid fraction (Fig. 7). It is clear from this figure that the local permeability is relatively close to $\kappa(\phi_R)$ over most of the aggregate volume,

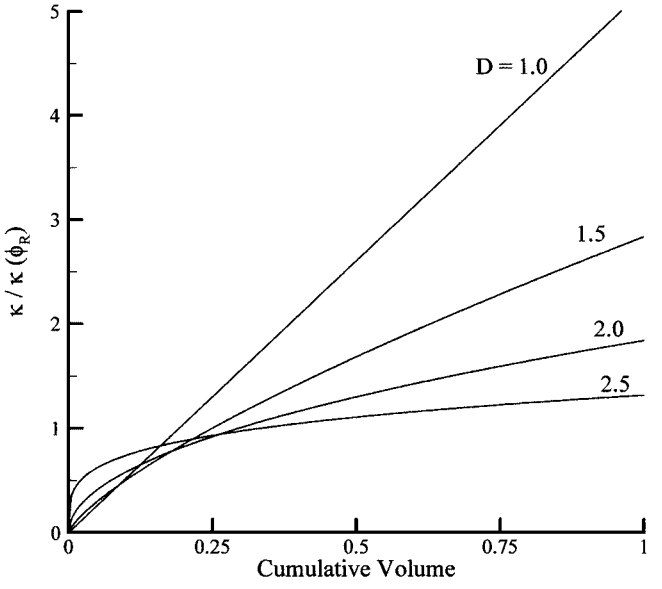

FIG. 7. The internal distribution of local permeability within an ideal fractal aggregate, normalized by the permeability associated with the average solid fraction, calculated using the Davies permeability expression for different values of the fractal dimension.

except for aggregates with $D < 1.5$. The volume averaged permeability κ_R is given in normalized form by

$$\frac{\kappa_R}{\kappa(\phi_R)} = \frac{\frac{3}{4\pi R^3}\int_0^{R_{max}}\kappa(\phi)4\pi r^2\,\mathrm{d}r}{\kappa(\phi_R)} = \frac{1}{1+0.5(3-D)}\left(\frac{3}{D}\right)^{1.5}. \qquad [25]$$

This ratio varies from 1.0 to 2.6 as the fractal dimension varies from 3.0 to 1.0, which is consistent with a similar analysis by Veerapaneni and Weisner (27).

The Davies expression for permeability may also be used to calculate the parameter $\beta = \frac{R}{\sqrt{\kappa}}$, which was defined earlier for a uniform aggregate. To apply this concept to a fractal aggregate with spatially varying properties, it is assumed that the uniform permeability is given by $\kappa = \kappa(\phi_R)$. This leads to the following expression for β:

$$\beta = 4\phi^{\frac{1}{D-3}+0.75}. \qquad [26]$$

For a typical range of solid fraction values, $0.001 < \phi_R < 0.05$, and for fractal dimensions ranging from 1.0 to 2.5, the value of β given by Eq. [26] is greater than 2 except for $D < 1.5$ (Fig. 8). This means that ideal aggregates with $D > 1.5$ are of the "effectively impermeable" type discussed earlier, i.e. the intercepted flow is small and the force on the aggregate is nearly that given by Stokes' Law for a sphere with the same radius ($\Omega \approx 1$). Even for the range $1 < D < 1.5$ the value of β is generally greater than 1. This finding is consistent with the

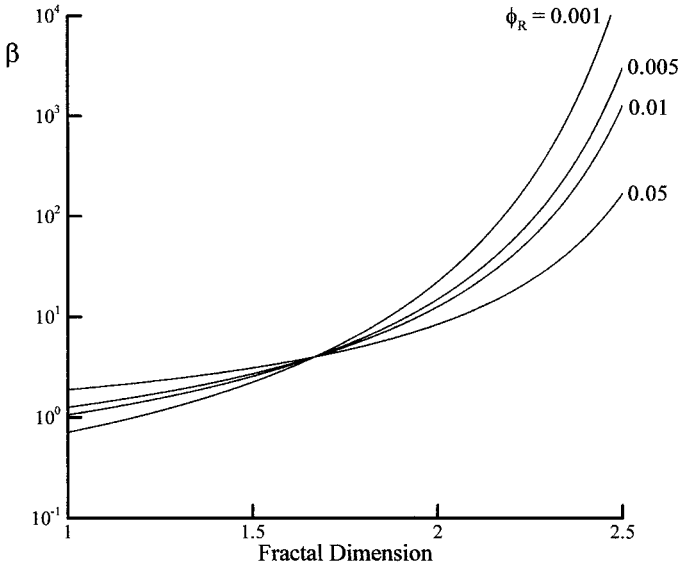

FIG. 8. The theoretical variation of the parameter β for an ideal fractal aggregate as a function of the aggregate average solid fraction ϕ_R and fractal dimension D using the Davies permeability expression.

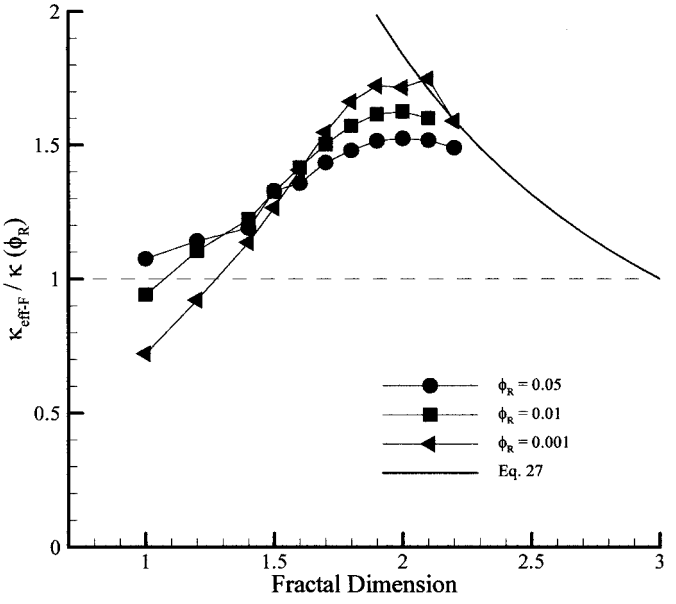

FIG. 9. The theoretical variation of the effective permeability of an ideal fractal aggregate as a function of the average solid fraction ϕ_R and fractal dimension D using the Davies permeability formulation. The symbols are the values obtained using the Brinkman equation and the solid line is an asymptotic relationship (Eq. [27]) valid as the fractal dimension approaches a value of 3.

observations of previous studies of fractal aggregates that have found $\beta > 1$ for living and nonliving fractal aggregates (6).

To evaluate the validity of the assumption that $\kappa \approx \kappa(\phi_R)$, the Brinkman equation was applied to ideal fractal aggregates with radially varying properties. Using Eq. [8], the "effective" permeability $\kappa_{eff\text{-}F}$ defined as the permeability of a uniform aggregate of the same size that gives the correct hydrodynamic force. Values of $\kappa_{eff\text{-}F}$ derived in this way are within 60% of $\kappa(\phi_R)$ for $0.001 < \phi_R < 0.05$ and $1.0 < D < 2.5$ (see Fig. 9). For a fixed value of ϕ_R the effective permeability obtains a maximum value greater than $\kappa(\phi_R)$ for D just less than 2.0. Theoretically, $\kappa_{eff\text{-}F}$ must decrease from this maximum and approach $\kappa(\phi_R)$ as $D \to 3$. This limit was not completely observed in the computed values of $\kappa_{eff\text{-}F}$ because the numerical application of the Brinkman equation was nonconvergent for $D > 2.2$. The decrease in $\kappa_{eff\text{-}F}$ for smaller values of D is thought to be associated with the corresponding decrease in β, which is accompanied by a penetration of the external flow further into the aggregate where it interacts with the region of smaller local permeability (see Fig. 7). Similar results were obtained for values of $\kappa_{eff\text{-}U}$, defined as the permeability of a uniform aggregate that gives the correct intercepted flow.

For $\beta \gg 1$ it is likely that the penetration of the external flow will be confined to a region near the aggregate surface where $\phi \approx \frac{D}{3}\phi_R$ (see Eq. [20]). This value of the solid fraction corresponds to a permeability given by

$$\kappa = \left(\frac{3}{D}\right)^{1.5} \kappa(\phi_R) \qquad [27]$$

This relationship appears to agree with the numerically computed values of $\kappa_{eff\text{-}F}$ for $D > 2$, although the comparison is limited by the lack of $\kappa_{eff\text{-}F}$ values as D approaches 3 (see Fig. 9).

Finally, it is reasonable to ask how well real aggregates correspond to the ideal aggregate model used in this section. As an example, the radial variation of $N(r)$ within the synthetic aggregate formed numerically by differential settling is shown in Fig. 10. Indicated on this figure are the values of the length

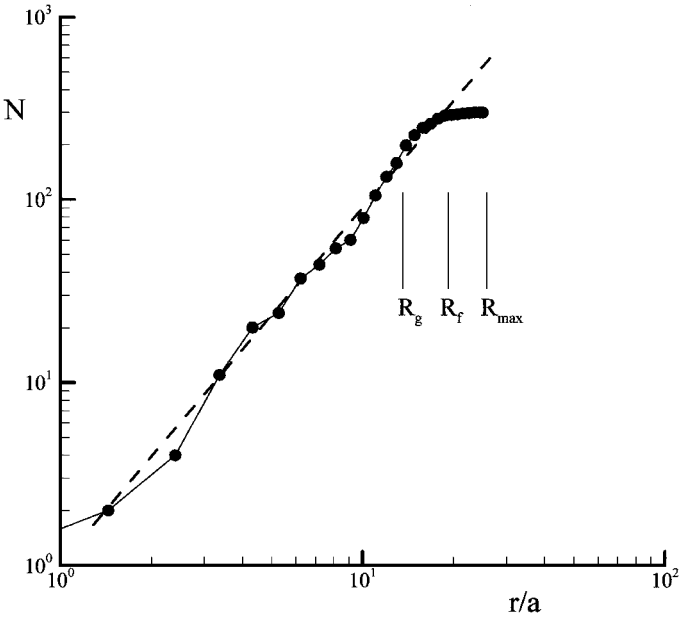

FIG. 10. The cumulative number of primary particles N as a function of the dimensionless radius r/a for the aggregate formed by differential settling (see Table 2). The slope of the dashed line is the fractal dimension D. Values of the average radius of gyration $R_g/a = 13.6$, the outer radius $R_f/a = 19.3$, and the maximum radius $R_{max}/a = 26.0$ are indicated.

scales R_g, R_f, and R_{max}, where R_f was defined from Eq. [3]. What is clear is that the ideal fractal structure given by Eq. [19] is valid over most of the radius of the aggregate, but that the outermost region, roughly corresponding to $R_f < r < R_{max}$, is very sparsely populated relative to the ideal structure.

This deviation from ideal structure at the outer edge of the aggregate manifests itself as an uncertainty in the effective size of the aggregate, because the value of R_{max} may be determined by a few isolated fragments of the aggregate that populate the sparse outer region but do not have much influence on the hydrodynamic force or interaction with the intercepted flow. In particular, this uncertainty in the aggregate size R can lead to significant errors in estimating the effective permeability of the aggregate from measurements of the hydrodynamic force F as determined by numerical analysis or observation of the aggregate settling velocity. In both cases the value of the parameter Ω defined in Eq. [8] is inversely proportional to the value of R. For $\beta \gg 1$, which is expected, small changes in Ω are associated with very large changes in β and thus in the estimate of the effective uniform permeability. For example, the aggregate formed by differential settling (see Table 2) has $R_h = 14.9a$ (for the Davies permeability relationship). If the length scale is $R_{max} = 26.0a$, then $\Omega = R_h/R_{max} = 0.57$ and $\beta = 2.8$, leading to $\kappa/a^2 = 86.2$. If the length scale for the aggregate is instead $R_f = 19.3a$, then $\Omega = 0.77$ and $\beta = 5.2$, leading to $\kappa/a^2 = 13.9$, which is significantly smaller than the value obtained using R_{max}.

The Clustered Aggregate Hypothesis

The synthetic fractal aggregates analyzed here provide a direct test of the hypothesis of Johnson and Logan (42) and Li and Logan (43, 44) that the particle size used in the permeability relationship should be effectively larger than the primary particles as a result of clustering of primary particles within the aggregate. For example, the third generation ($k = 3$) synthetic random lattice-based aggregate with $n_l = 5$, $n_p = 13$, $D_f = 1.59$, and a primary particle size a can be "replaced" by a second-generation ($k = 2$) structure, also with $n_l = 5$, $n_p = 13$, and $D_f = 1.59$, by simply representing the smallest clusters in the third-generation aggregate by a unit particle of size $n_l a = 5a$ (see Fig. 11). The physical properties of these two aggregates computed using the Davies relationship are compared in Table 4. It is clear from this comparison that the aggregate with clustered particles actually has lower permeability and a smaller settling velocity ratio (the settling velocity of the permeable aggregate divided by the velocity of an impermeable aggregate with the same bulk density $= \Omega^{-1}$) than the clustered aggregate. The reason for this is that considering the clustered regions to act as impermeable units implies an increase in the solid fraction, corresponding to "filling" the void spaces in the clusters. This increase in solid fraction results in a predicted increase in the quantity κ/a^2, regardless of which permeability relationship is used. For the aggregate used in this example and for the Davies permeability relationship, the effect of this increase in the solid fraction counteracts the increase in the effective primary particle size.

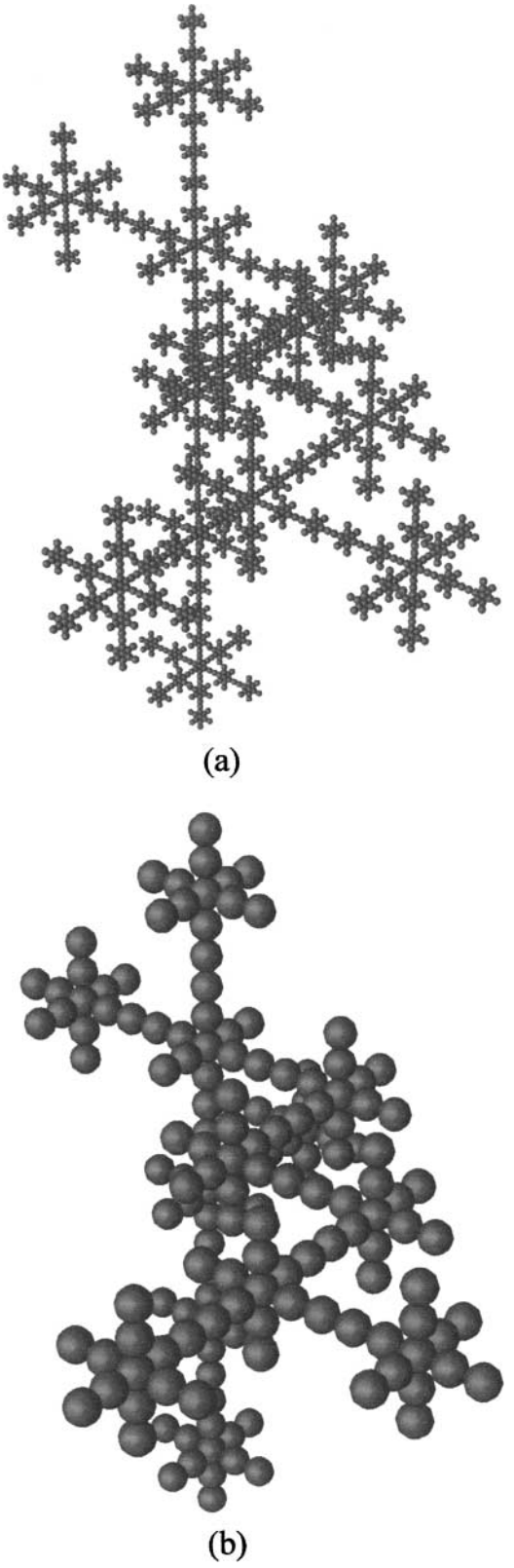

FIG. 11. Comparison of (a) a synthetic lattice aggregate of third generation ($k = 3$ and $n_l = 5$) with $N_R = 2197$ primary particles of size a with (b) a synthetic aggregate in which the primary particles of the aggregate in (a) have been clustered into $N_c = 167$ clusters of size $5a$ (see Table 4).

TABLE 4
Calculated Permeability and Other Parameters of Lattice Aggregates with the Same Structure but Different Levels of Clustering

Aggregate type	R_{max}	N_R	N_c	a	ϕ_R	κ/a^2	κ	β	Ω^{-1}
Lattice aggregate with $n_l = 5$, $k = 3$, and $a = 1$ (see Table 2 and Fig. 11)	160	2197	2197	1	0.00054	4980	4980	2.27	2.05
Lattice aggregate with $n_l = 5$, $k = 2$, and $a = 5$ (see Table 2 and Fig. 11)	160	2197	169	5	0.0052	167	4170	2.48	1.90

Note. Values of κ/a^2 are calculated using the Davies formula (see Table 1); values of R_{max} and κ are in the same units as the primary particle length.

It is clear from this example that clustering within an aggregate cannot in general explain experimentally high sinking velocities.

A wider range of aggregate properties can be investigated using the approach of Li and Logan (44) in which the effect of clustering within an ideal fractal aggregate is demonstrated simply by plotting the settling velocity ratio versus the number of clusters in the aggregate N_c, keeping the fractal dimension D constant and assuming that N_c is related to R_{max} and D by Eq. [1]. As previously discussed, specification of two aggregate properties, in this case the number of clusters and the fractal dimension, is sufficient to determine all the aggregate characteristics such as solid fraction, etc. A large value of N_c represents a relatively unclustered aggregate; conversely, N_c decreases as the extent of clustering increases. For every value of N_c the aggregate solid fraction and dimensionless size R_{max}/a are determined and these values can be used, in conjunction with a chosen permeability relationship, to calculate the value of $\Omega(\beta)$ and thus the velocity ratio (see Li and Logan (44) for details). The results of such an analysis are shown in Fig. 12, which reproduces the curves shown in Fig. 4 of Li and Logan (44) for $D = 1.7$ and $D = 2.5$, using their value $A = 0.25$ in Eq. [1] and the Brinkman permeability relationship. Shown for comparison are the velocity ratios calculted using the Davies permeability relationship for the same fractal dimensions and also for $D = 1.59$ using both permeability functions. It is clear that the change in the velocity ratio with increased clustering within the aggregate depends on the choice of permeability relationship in conjunction with the value of the fractal dimension. The result of $D = 1.59$ using the Brinkman equation indicates an increase of the velocity ratio with increasing clustering (decreasing N_c). If the Davies equation is used with $D = 1.59$, just the opposite result is obtained, consistent with the example above (see Table 4). The velocity ratio for $D = 1.7$ obtained using the Davies relationship remains in the range 2–3 even as N_c increases by several orders of magnitude, indicating that for ideal fractal aggregates clustering is theoretically not necessary to obtain velocity ratios on the order of those observed by Li and Logan (43).

If, as demonstrated by this study, the Davies permeability relationship is more valid for fractal aggregates than the Brinkman relationship and provides good permeability estimates for synthetic fractal aggregates such as those used in the example above, why does it fail to predict the velocity ratio for the actual aggregates used by Li and Logan (43) without invoking clustering? The answer is that the aggregates used in the experimental work of Li and Logan (43) were probably not fractal aggregates in the sense of being characterized by a single fractal dimension at all scales within the aggregate. This can be demonstrated by choosing as an example the aggregates in the "A" series of Li and Logan's experiment, which was found to have a fractal dimension $D = 1.81$ based on the variation of solid volume with aggregate size within the population of aggregates studied. From Fig. 2 in Li and Logan (43) it can be seen that an aggregate in this series with radius $R_{max} = 150$ μm has a total solid volume $V_a = 10^6$ μm^3. The average solid fraction of the aggregate is then $\phi_R = \frac{V_a}{\frac{4}{3}\pi R_{max}^3} = 0.071$. Considering that the primary particles have a radius $a = 1.43$ μm, the total number of primary particles in the aggregate must be $N_R = \frac{V}{\frac{4}{3}\pi R_{max}^3} = 82{,}502$. The

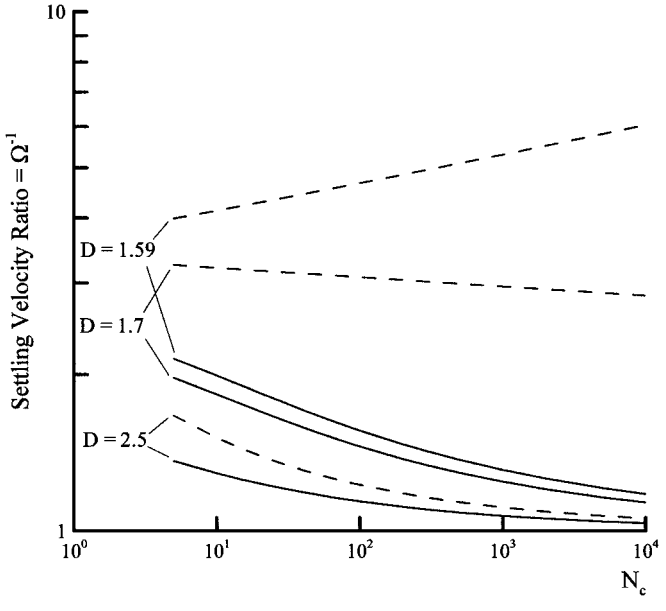

FIG. 12. The variation of the theoretical settling velocity ratio (the ratio of the settling velocity of a permeable aggregate to that of an impermeable aggregate with the same size and mass) for ideal fractal aggregates with N_c clusters, for three different values of the fractal dimension D, and for two different permeability expressions (Brinkman, solid lines; Davies, dashed lines). To be comparable with Li and Logan (43), these calculations are based on Eq. [1] with a prefactor value $A = 0.25$.

conclusion that this aggregate is not fractal in the ideal sense is based on Eq. [1], which requires that $N_R = A(\frac{R_{max}}{a})^D = 4545$, using $A = 1$. Li and Logan (43) used $A = 0.25$, which results in $N_R = 1136$. To match the actual value $N_R = 82,502$ requires either that $A = 18.2$, which is far larger than expected for an ideal fractal aggregate, or that, for the individual aggregate, $D = 2.43$, which is significantly larger than the population-based value of 1.81. A nonfractal structure would explain why the experimental aggregates with a radius of 150 μm and a fractal dimension of 1.81 could have a volume fraction as high as 0.07, in contrast with most other measurements on aggregates of this size and fractal dimension (see 12). Similar results, not shown here, are obtained from an analysis of the experiments of Johnson and Logan (42).

In the experiments of Li and Logan (43) the aggregates were apparently either formed by aggregation of clusters with a different fractal dimension than the overall aggregate, or the internal structures of the aggregates were reworked subsequent to formation of the aggregate. There are no actual measurements of the internal structure of the experimental aggregates used by Li and Logan (43), so it is impossible to say definitively in what way the internal structure differs from that of a fractal aggregate or how the nonfractal structure affected the observed aggregate sinking speeds. However, the analysis of clustering presented above indicates that, although clustering may not be necessary to explain higher sinking velocities for all combinations of aggregate parameters, it is clearly sufficient for many cases. Thus it is possible to conclude that, as hypothesized by Li and Logan (43, 44) and Johnson and Logan (42), the formation of low-permeability clusters affected the aggregate permeability and sinking speed of the experimental aggregates significantly, but not in a way predicted by an ideal fractal model.

Future Work

The experimental aggregates used by Li and Logan (43) and Johnson and Logan (42) demonstrated fractal behavior in terms of the variation of aggregate solid volume with aggregate size within the population of the aggregates studied, but not within individual aggregates. This may be a characteristic of experimental aggregates characterized only at the population level in many others studies. Progress in understanding important aggregate properties such as permeability will depend upon advances in our ability to observe the structure of individual aggregates.

The need for future work using the simulation tools described here lies in several areas. Real aggregates are composed of polydisperse primary particles and it should be straightforward to generate and simulate such aggregates. Additional simulations of aggregates with more "realistic" structures using differential settling, turbulent shear, or other physical aggregation mechanisms would provide additional insights.

REFERENCES

1. Rosner, D. E., and Pushkar, T., *AIChE J.* **40,** 1167 (1994).
2. Filippov, A. V., Zurita, M., and Rosner, D. E., *J. Colloid Interface Sci.* **229,** 261 (2000).
3. Neale, G., Epstein, N., and Nader, W., *Chem. Eng. Sci.* **28,** 1865 (1973).
4. Logan, B. E., and Hunt, J. R., *Limnol. Oceanogr.* **32,** 1034 (1987).
5. Stolzenbach, K. D., Newman, K. A., and Wong, C. S., *J. Geophys. Res.* **97,** 17 (1992).
6. Stolzenbach, K. D., *Deep-Sea Res.* **40,** 359 (1993).
7. Adler, P. M., and Mills, P. M., *J. Rheol.* **23,** 25 (1979).
8. Sonntag, R. C., and Russel, W. B., *J. Colloid Interface Sci.* **115,** 387 (1987).
9. Meakin, P., *Rev. Geophys.* **29,** 317 (1991).
10. Wu, M. K., and Friedlander, S. K., *J. Colloid Interface Sci.* **159,** 246 (1993).
11. Sorensen, C. M., and Roberts, G. C., *J. Colloid Interface Sci.* **186,** 447 (1997).
12. Logan, B. E., and Wilkinson, D. B., *Limnol. Oceanogr.* **35,** 130 (1990).
13. Rogak, S. N., and Flagan, R. C., *J. Colloid Interface Sci.* **134,** 206 (1990).
14. Rogak, S. N., and Flagan, R. C., *J. Colloid Interface Sci.* **151,** 203 (1992).
15. Brinkman, H. C., *Appl. Sci. Res.* **A1,** 27 (1947).
16. Happel, J., and Brenner, H., "Low Reynolds Number Hydrodynamics," Kluwer, Dordrecht, 1991.
17. Happel, J., *AIChE J.* **4,** 197 (1958).
18. Howells, I. D., *J. Fluid. Mech.* **64,** 449 (1974).
19. Hinch, E. J., *J. Fluid Mech.* **83,** 695 (1977).
20. Kim, S., and Russel, W. B., *J. Fluid Mech.* **154,** 269 (1985).
21. Neale, G. H., and Nader, W. K., *AIChE J.* **20,** 530 (1974).
22. Brinkman, H. C., *Appl. Sci. Res.* **A1,** 81 (1947).
23. Jackson, G. W., and James, D. F., *Can. J. Chem. Eng.* **64,** 364 (1986).
24. Davies, C. N., *Proc. Inst. Mech. Eng.* **B1,** 185 (1952).
25. Drummond, J. E., and Tahir, M. I., *Int. J. Multiphase Flow* **10,** 515 (1984).
26. Higdon, J. J. L., and Ford, G. D., *J. Fluid Mech.* **308,** 241 (1996).
27. Veerapaneni, S., and Wiesner, M. R., *J. Colloid Interface Sci.* **177,** 45 (1996).
28. Ooms, G., Mijnlieff, P. F., and Beckers, H., *J. Chem. Phys.* **53,** 4123 (1970).
29. Filippov, A. V., *J. Colloid Interface Sci.* **229,** 184 (2000).
30. Brady, J. F., and Bossis, G., *Annu. Rev. Fluid Mech.* **20,** 111 (1988).
31. Durlofsky, L., Brady, J. F., and Bossis, G., *J. Fluid Mech.* **180,** 21 (1987).
32. Ganatos, P., Pfeffer, R., and Weinbaum, S., *J. Fluid Mech.* **84,** 79 (1978).
33. Hassonjee, Q., Ganatos, P., and Pfeffer, R., *J. Fluid Mech.* **197,** 1 (1988).
34. Durlofsky, L., and Brady, J. F., *Phys. Fluids* **30,** 3329 (1987).
35. Bossis, G., Meunier, A., and Brady, J. F., *J. Chem. Phys.* **94,** 5064 (1991).
36. Vitthal, S., and Sharma, M. M., *J. Colloid Interface Sci.* **153,** 314 (1992).
37. Mazur, P., and Van Saarloos, W., *Physica* **115A,** 21 (1982).
38. Matsumoto, K., and Suganuma, A., *Chem. Eng. Sci.* **32,** 445 (1977).
39. Masliyah, J. H., and Polikar, M., *Can. J. Chem. Eng.* **58,** 299 (1980).
40. Li, D. H., and Ganczarczyk, J., *Water Environ. Res.* **64,** 236 (1992).
41. Lasso, I. A., and Weidman, P. D., *Phys. Fluids* **20,** 3921 (1986).
42. Johnson, C. P., Li, X., and Logan, B. E., *Environ. Sci. Technol.* **30,** 1911 (1996).
43. Li, X., and Logan, B. E., *Environ. Sci. Technol.* **31,** 1229 (1997).
44. Li, X., and Logan, B. E., *Water Res.* **35,** 3373 (2001).
45. Kim, S., "Dynamics of Particle Accumulation at Engineered and Natural Interfaces," Ph.D. thesis, Civil and Environmental Engineering, University of California, Los Angeles, 2000.
46. Philips, R. J., Brady, J. F., and Bossis, G., *Phys. Fluids* **31,** 3462 (1988).
47. Blackford, L. S., Choi, J., Cleary, A., D′Azevedo, E., Demmel, J., Chillon, I., Dongarra, J., Hammarling, D., Henry, G., Petitet, A., Stanley, K., Walker, D., and Whaley, R. C., "ScaLAPACK User's Guide," SIAM, Philadelphia, 1997.
48. Cichocki, B., and Hinsen, K., *Phys. Fluids* **V7,** 285 (1994).